14th European Conference on Applied Superconductivity (EUCAS 2019) IOP Publishing
Journal of Physics: Conference Series **1559** (2020) 012029 doi:10.1088/1742-6596/1559/1/012029

Simulation of mechanical stresses in reinforced REBaCuO disk bulks during pulsed-field magnetization

F. Shimoyashiki[1], H. Fujishiro[1], T. Hirano[1], T. Naito[1], M. D. Ainslie[2]

[1] Department of Physical Science and Materials Engineering, Faculty of Science and Engineering, Iwate University, Morioka 020-8551, Japan
[2] Bulk Superconductivity Group, Department of Engineering, University of Cambridge, Trumpington Street, Cambridge CB2 1PZ, UK

E-mail: fujishiro@iwate-u.ac.jp

Abstract. We have performed numerical simulations of the electromagnetic hoop stress, σ_θ, in a REBaCuO disk bulk reinforced by a metal ring during pulsed-field magnetization (PFM) using a solenoid coil, in which the superconducting characteristics of the bulk material were assumed to have realistic J_c-B-T ones. The compressive and tensile σ_θ stresses were applied in the bulk during the ascending and descending stages of PFM, respectively. The time and position dependences of the mechanical stresses were estimated. The possibility of mechanical fracture due to these hoop stresses and the effect of the metal ring reinforcement were discussed.

1. Introduction

It is important to enhance the trapped magnetic field in RE-Ba-Cu-O (REBaCuO, RE: rare earth element or Y) superconducting bulks because the high-field trapped field magnet (TFM) is capable of generating several Tesla. Although the trapped field estimated from its critical current density $J_c(B, T)$ could theoretically be over 30 T at 29 K [1], the mechanical strength of the brittle ceramic material restricts the maximum trapped field experimentally. A trapped field of 17.24 T has been achieved at 29 K in a YBaCuO disk bulk pair by mechanical reinforcement of resin impregnation and carbon fiber wrapping [1]. To date, the highest trapped field of 17.6 T has been achieved at 26 K in a GdBaCuO disk bulk pair reinforced by shrink-fit stainless steel [2], both of which were magnetized by field-cooled magnetization (FCM). Analytical investigations of mechanical properties were reported for disk- and ring-shaped bulks with infinite height during FCM or zero-field-cooled magnetisation (ZFCM) [3 – 6]; the results were primarily based on Bean's critical state model with constant J_c characteristics. We have performed the numerical simulation of electromagnetic, thermal properties and mechanical stresses (hoop stress, σ_θ, and radial stress, σ_r) in REBaCuO disk and ring bulks with finite height reinforced by metal ring during FCM using finite element method (FEM) [7 - 11], in which the mechanical stresses and reinforcement of disk bulks during FCM and the cooling process were investigated [9].

The pulsed-field magnetization (PFM) is a practical magnetizing technique to realize TFMs without the need for a superconducting magnet, in contrast to FCM, because of its relatively compact, inexpensive, and mobile experimental setup [12 - 16]. However, the trapped field by PFM is much lower than that by FCM because of a large temperature rise due to the rapid and dynamic motion of magnetic flux. The trapped field of 5.20 T has been achieved on a GdBaCuO bulk 45 mm in diameter at 30 K using a modified multi-pulse technique with stepwise cooling (MMPSC) [15], which is a record-high

trapped field for REBaCuO bulk by PFM to date. However, there were experimentally few evidences of the mechanical fracture during PFM. The stress analyses by numerical simulation during PFM have been reported, in which the disk bulk was not reinforced by metal ring [17]. However, it is necessary to clarify the mechanical stress for the bulk reinforced by metal ring, which is a usual setup during magnetization process.

In this paper, based our experience for the mechanical analysis during FCM, the time and position dependences of the electromagnetic hoop stress, σ_θ, along the circumferential direction are estimated for the disk bulk reinforced by a stainless steel ring during PFM. The possibility of mechanical fracture due to the compressive and tensile stresses and the effect of the metal ring reinforcement are discussed.

2. Numerical simulation procedure

Based on our experimental setup [12 - 16], a three dimensional (3D) numerical model coupling the electromagnetic, thermal and mechanical properties was constructed. The REBaCuO disk bulk (65 mm in outer diameter (O.D.) and 20 mm in height (H)) was mounted in a stainless steel (SUS) ring holder of 5 mm in thickness (75 mm in O.D. and 65 mm in I.D.) with the same height and was thermally connected to the cold stage using a thin indium sheet, as shown in Fig. 1(a). The disk bulk was magnetized using a coil (121 mm in O.D., 95 mm in I.D. and 50 mm in H). The applied pulsed field, $B_{ex}(t)$, with the rise time of 13 ms and the duration time of 200 ms was applied, in which the magnitude of pulsed field, B_{ex}, was changed from 3.5 to 6.0 T. The initial temperature, T_s, was set to T_s = 65 K. The following magnetic field dependence of $J_c(B)$, proposed by Jirsa, was used in the simulation [18],

$$J_c(B) = J_{c1}\exp\left(-\frac{B}{B_L}\right) + J_{c2}\frac{B}{B_{max}}\exp\left[\frac{1}{k}\left(1-\left(\frac{B}{B_{max}}\right)^k\right)\right]. \quad (1)$$

The experimental $J_c(B, T)$ data were fit up to 10 T between 60, 65, 70 and 77 K using eq. (1), as shown in Fig. 1(b), and the parameters were determined at each temperature [19]. For example, each parameter value at 65 K was $J_{c1} = 1.17 \times 10^9$ A/m^2, $B_L = 0.57$ T, $J_{c2} = 7.56 \times 10^8$ A/m^2, $B_{max} = 3.0$ T and $k = 1.3$. The $J_c(B, T)$ profiles at intermediate magnetic fields and temperatures are interpolated based on each parameter [19]. The commercial software packages, Photo-Eddy, combined with Photo-Thermo (Photon Ltd, Japan), were used for the analysis.

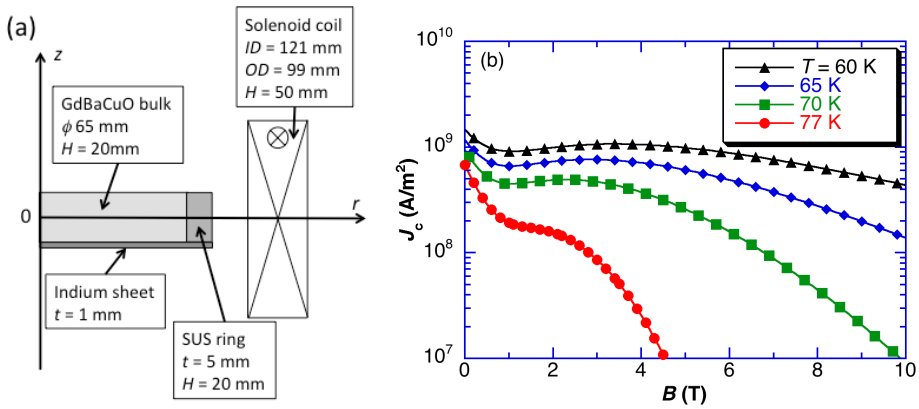

Figure 1. (a) A schematic view of the disk bulk and the stainless steel ring, which is magnetized by the solenoid coil. (b) The $J_c(B, T)$ profiles of the REBaCuO bulk at 60, 65, 70 and 77 K, used in the numerical simulation.

Table 1. Mechanical parameters (Young's modulus, E_Y, Poisson ratio, ν, and average thermal expansion coefficient, α_{av}) of REBaCuO bulk, stainless steel and indium used in the simulation.

	E_Y (GPa)	ν	α_{av} (K^{-1})
REBaCuO bulk	100	0.33	6.80×10^{-6}
stainless steel (SUS)	78	0.34	1.72×10^{-5}
indium	12.7	0.34	1.60×10^{-5}

Elastic behaviour in an isotropic material can be explained by Hooke's law. The electromagnetic hoop stress, σ_θ, was numerically simulated. The detailed procedure of the mechanical analysis used in this study has been shown elsewhere [7, 10]. The nodal force on each node of the meshed element calculated by Photo-Eddy was exported to the commercial software package Photo-ELAS (Photon Ltd., Japan) for analysis of the electromagnetic stress. The mechanical parameters (Young's modulus, E_Y, Poisson ratio, ν, and the average thermal contraction coefficient, α_{av}) of the REBaCuO bulk, SUS ring, and indium are summarised in table 1. The mechanical parameters of the REBaCuO bulk were assumed to be isotropic and homogeneous for simplicity, and typical values of the *ab*-plane were used.

3. Results and discussion

Fig. 2(a) shows the time dependence of the applied pulsed field, $B_{ex}(t)$, of 6.0 T used in the simulation and the simulation result of the trapped field, $B_z(t)$, at the center of the bulk ($r = z = 0$ mm) at $T_s = 65$ K. The magnetic flux intruded into the bulk center a little later and then the trapped field gradually decreased due to the flux creep. Figs. 2(b) and 2(c), respectively, show the measured and calculated final trapped field, B_z, on the center of the bulk surface ($r = 0$ mm, $z = 10.5$ mm) at $t = 7$ s, and the maximum temperature rise, ΔT_{max}, on the edge of the bulk surface ($r = 32$ mm, $z = 10.5$ mm), as a function of applied pulsed field, B_{ex}. The experimental results are also shown [14], which were reproduced by the simulation quantitatively. The B_z value took a maximum and then decreased with increasing B_{ex}. The ΔT_{max} value monotonically increased with increasing B_{ex}.

Figs. 3(a) and 3(b) show the simulation results of ascending and descending stages of the trapped field profiles, $B_z(z = 0$ mm), after applying the pulsed field of $B_{ex} = 5.5$ T. Figs. 3(c) and 3(d), respectively, show the trapped field profiles at $t = 13$ ms (pulse peak) and $t = 9$ s (final). In the ascending stage, the magnetic flux gradually penetrated from the bulk periphery and surface as shown in Fig. 3(c). In the descending stage, the magnetic flux intruded abruptly like a flux jump to the bulk center at $t = 20$ ms due to the reduction of the pinning force by the temperature rise. Finally, the cone-shaped trapped field profile was obtained as shown in Fig. 3(d).

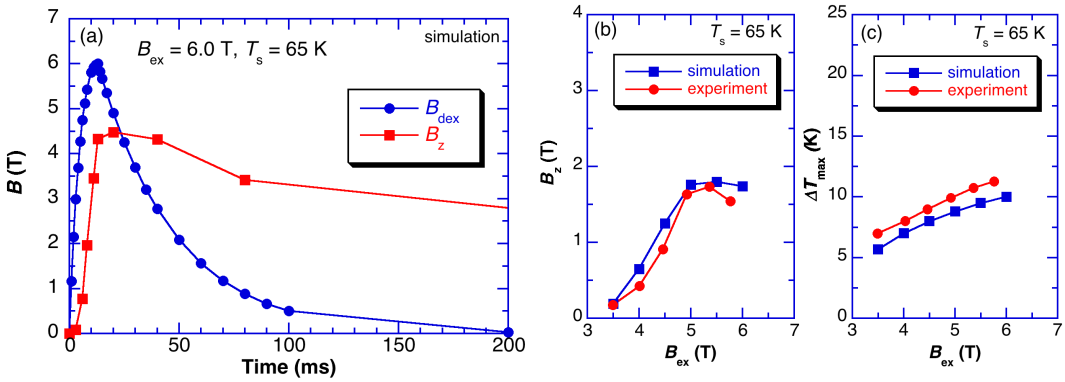

Figure 2. (a) Time dependence of the applied pulsed field, $B_{ex}(t)$, of 6.0 T, and of the trapped field, $B_z(t)$, at the center of the bulk ($r = z = 0$) at $T_s = 65$ K. (b) The experimental and numerical results of the trapped field, B_z, on the surface of the bulk center and (c) the maximum temperature rise, ΔT_{max}, in the bulk, as a function of applied pulsed field, B_{ex}.

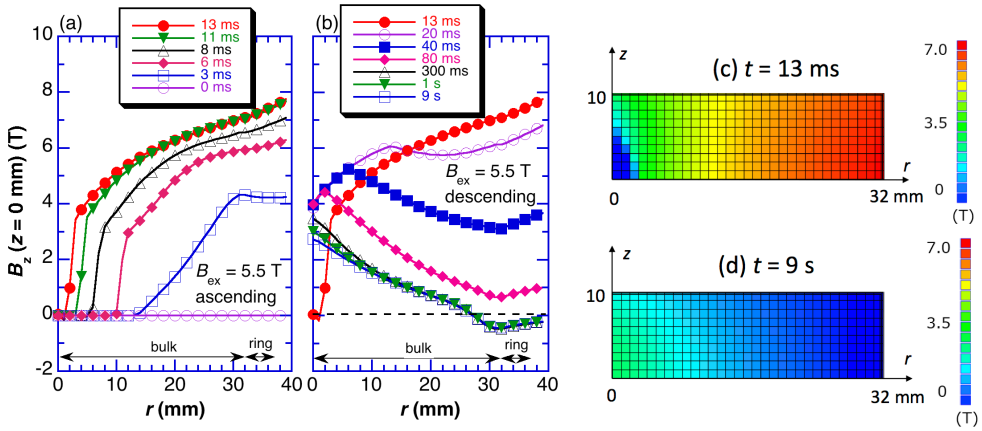

Figure 3. The simulation results of time evolution of the (a) ascending and (b) descending stages of the trapped field profiles, $B_z(z = 0$ mm), after applying the pulsed field of $B_{ex} = 5.5$ T at 65 K. The cross sections of the trapped field profiles at (c) $t = 13$ ms (pulse peak) and (d) $t = 9$ s (final).

Figs. 4(a) and 4(b) show the time evolution of the temperature profiles, $T(z = 0$ mm), in the ascending and descending stages, after applying the pulsed field of $B_{ex} = 5.5$ T. Figs. 4(c) and 4(d), respectively, show the temperature profiles at $t = 13$ ms and $t = 9$ s. In the ascending stage, the temperature increased gradually from the bulk periphery due to the flux penetration, as shown in Fig. 3(c). In the descending stage, the generated heat mainly diffused toward the bulk center and was removed by the cold stage. As a result, the temperature was decreased and equalized at $t = 9$ s, as shown in Fig. 4(d).

Figs. 5(a) and 5(b) show the time evolution of the electromagnetic hoop stresses, $\sigma_\theta(z = 0$ mm), in the ascending and descending stages, after applying the pulsed field of $B_{ex} = 5.5$ T at 65 K. Figs. 5(c) and 5(d), respectively, show the σ_θ profiles at $t = 13$ ms and $t = 9$ s. In the ascending stage, the electromagnetic stress negatively increased with increasing time and the compressive stress, which was as large as -15 MPa at $t = 13$ ms, was the largest at the bulk center, as shown in Fig. 5(c). The compressive stress was also applied to the SUS ring. In the descending stage, the compressive stress changes to the tensile stress with increasing time. The maximum tensile stress of + 7 MPa was applied at $t = 40$ ms and then the final tensile stress at $t = 9$ s was lower than +5 MPa, as shown in Fig. 5(d).

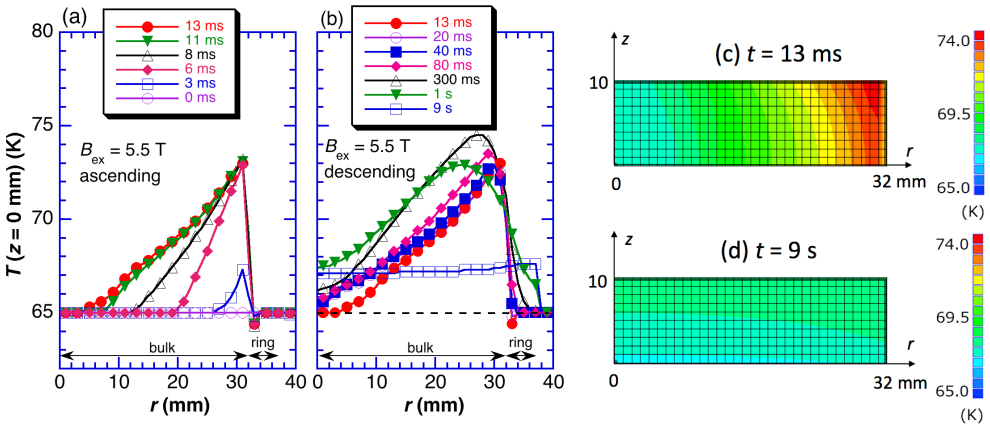

Figure 4. The time evolution of the (a) ascending and (b) descending stages of the temperature profiles, $T(z = 0$ mm), after applying the pulsed field of $B_{ex} = 5.5$ T. The cross sections of temperature profiles at (c) $t = 13$ ms (pulse peak) and (d) $t = 9$ s (final).

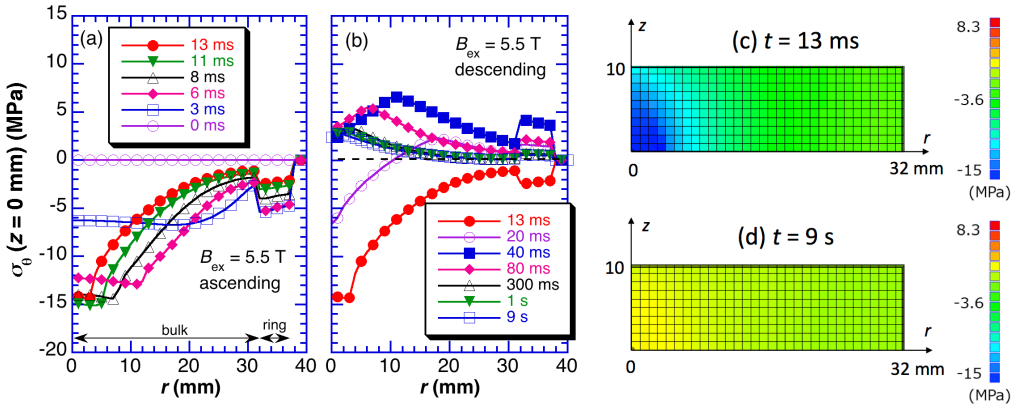

Figure 5. The time evolution of the (a) ascending and (b) descending stages of the electromagnetic stress profiles, $\sigma_\theta(z = 0$ mm), during the pulsed field of B_{ex} = 5.5 T at 65 K. The cross sections of the σ_θ profiles at (c) t = 13 ms (pulse peak) and (d) t = 9 s (final).

Fig. 6(a) shows the time evolution of the maximum electromagnetic hoop stress, σ_θ^{max}, at z = 0 and 10 mm in the disk bulk in the ascending and descending stages, during the applied pulsed field of B_{ex} = 5.5 T. The time evolution of the applied field, $B_{ex}(t)$ is also shown. The compressive stress took a maximum at t = 13 ms, and then changed to the tensile stress at t > 40 ms. The compressive stress at the bulk center (z = 0) is negatively larger than that at the bulk surface (z = 10 mm). Fig. 6(b) shows the maximum electromagnetic hoop stress, σ_θ^{max}, in the disk bulk in the ascending and descending stages, as a function of the applied pulsed field, B_{ex}. In both stages, the σ_θ^{max} value increases with increasing B_{ex} and the σ_θ^{max} value was as large as -17 MPa and +8 MPa in the ascending and descending stages, respectively. These σ_θ^{max} values are fairly smaller than the mechanical strength of the ReBaCuO bulk, which is as large as several hundred MPa for the compressive stress [21, 22] and 50 to 70 MPa for the tensile stress [22, 23]. When the operating temperature, T_s, decreases and the applied field, B_{ex}, increases, the σ_θ^{max} value would increase more.

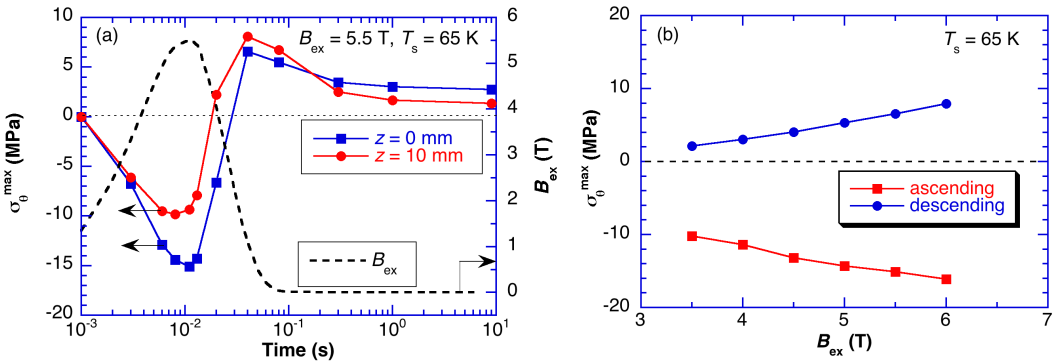

Figure 6. (a) The time evolution of the maximum electromagnetic stress, σ_θ^{max}, at z = 0 and 10 mm in the disk bulk in the ascending and descending stages, during the applied pulsed field of B_{ex} = 5.5 T at 65 K. (b) The maximum electromagnetic stress, σ_θ^{max}, in the disk bulk in the ascending and descending stages, as a function of the applied pulsed field, B_{ex}.

We have also performed the numerical simulation of the mechanical stress along the radial direction, σ_r. Figs. 7(a) and 7(b) show the time evolution of the electromagnetic hoop stresses, $\sigma_r(z = 0$ mm), in the ascending and descending stages, after applying the pulsed field of $B_{ex} = 5.5$ T at 65 K. The trends are similar to σ_θ along the circumferential direction. In the actual PFM experiments, the bulk with SUS ring is cooled from room temperature to the starting temperature, T_s. An additional thermal compressive stress is applied to the bulk from the SUS ring due to the difference of thermal expansion coefficient between REBaCuO bulk and SUS, which also protects the mechanical fracture. Actually, we have performed the PFM experiments several thousands of times for the disk bulks. However, we have never experienced the mechanical fracture of the disk bulk during PFM experimentally. The simulation results in this study are reasonable and support the experimental evidences.

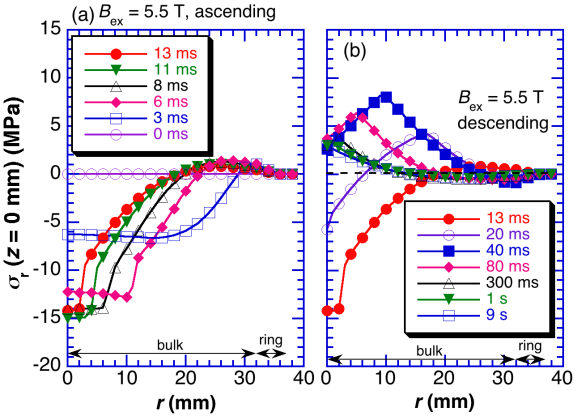

Figure 7. The time evolution of the (a) ascending and (b) descending stages of the electromagnetic stress profiles, $\sigma_r(z = 0$ mm), during the pulsed field of $B_{ex} = 5.5$ T at 65 K.

4. Summary

We have performed numerical simulations of the electromagnetic hoop stress, σ_θ, in a REBaCuO disk bulk reinforced by a SUS ring during PFM, in which the superconducting characteristics of the bulk material were assumed to have realistic J_c-B-T ones. The compressive and tensile σ_θ were applied in the bulk during the ascending and descending stages of PFM, respectively. The maximum σ_θ values were reasonably smaller than the fracture strength of the ReBaCuO bulk for the present experimental condition. If the operating temperature, T_s, decreases to 40 – 20 K and the applied field, B_{ex}, increases to 10 T, the σ_θ value will increase, but the disk bulk should never break during PFM. The simulation results in this study are reasonable and support the experimental evidence.

Acknowledgments

This research is partially supported by the Japan Society for the Promotion of Science (JSPS) KAKENHI Grant No. 15K04646. Mark Ainslie would like to acknowledge financial support from an Engineering and Physical Sciences Research Council (EPSRC) Early Career Fellowship EP/P020313/1. All data are provided in full in the results section of this paper.

References

[1] Tomita M and Murakami M 2003 *Nature* **421** 517
[2] Durrell J H, Dennis A R, Jaroszynski J, Ainslie M D, Palmer K G B, Shi Y-H, Campbell A M, Hull J, Strasik M, Hellstrom E E and Cardwell D A 2014 *Supercond. Sci. Technol.* **27** 082001
[3] Johansen T H, Chen Q Y and Chu W-K 2001 *Physica C* **349** 201
[4] Ren Y, Weinstein R, Liu J, Sawh R P and Foster C 1995 *Physica C* **251** 15
[5] Johansen T, Wang C, Chen Q Y and Chu W–K 2000 *J. Appl. Phys.* **88** 2730

[6] Johansen T 2000 *Supercond. Sci. Technol.* **13** R121
[7] Fujishiro H, Ainslie M D, Takahashi K, Naito T, Yanagi Y, Itoh Y and Nakamura T 2017 *Supercond. Sci. Technol.* **30** 085008
[8] Takahashi K, Fujishiro H, Naito T, Yanagi Y, Itoh Y and Nakamura T 2017 *Supercond. Sci. Technol.* **30** 115006
[9] Ainslie M D, Huang K Y, Fujishiro H, Chaddock J, Takahashi K, Namba S, Cardwell D A and Durrell J H 2019 *Supercond. Sci. Technol.* **32** 015007
[10] Takahashi K, Namba S, Fujishiro H, Naito T, Yanagi Y, Itoh Y and Nakamura T 2019 *Supercond. Sci. Technol.* **32** 015007
[11] Fujishiro H, Naito T, Yanagi Y, Itoh Y and Nakamura T 2019 *Supercond. Sci. Technol.* **32** 065001
[12] Fujishiro H, Naito T, Kakehata K, Yanagi Y and Itoh Y 2010 *Supercond. Sci. Technol.* **23** 025013
[13] Ainslie M D and Fujishiro H 2015 *Supercond. Sci. Technol.* **28** 053002
[14] Shimoyashiki F, Fujishiro H, Naito T, and Ainslie M D 2019 *IEEE Trans. Appl. Supercond.* **29** 6802405
[15] Fujishiro H, Tateiwa T, Fujiwara A, Oka T and Hayashi H 2006 *Physica C* **445-448** 334
[16] Mochizuki H, Fujishiro H, Naito T, Itoh Y, Yanagi Y and Nakamura T 2016 *IEEE Trans. Appl. Supercond.* **26** 6800205
[17] Wu H, Yong H and Zhou Y 2018 *Supercond. Sci. Technol.* **31** 045008
[18] Jirsa M, Ůust L, Dlouhý D and Koblischka M R 1997 *Phys. Rev. B* **55** 3276
[19] Hirano T, Takahashi K, Shimoyashiki F, Fujishiro H, Naito T, and Ainslie M D 2019 *IEEE Trans. Appl. Supercond.* **29** 8000705
[20] Kan R, K Katagiri K, Murakami A, Kasaba K, Shoji Y, Noto K, Sakai N and Murakami M 2004 *IEEE Trans. Appl. Supercond*. **14** 8132078
[21] Murakami A, Katagiri K, Kan R, Miyata H, Shoji Y, Noto K, Iwamoto A and Mito T 2005 *Physica C* **426–431** 644
[22] Lee D and Salama K 1990 Japan. *J. Appl. Phys.* **29** L2017
[23] Katagiri K, Murakami A, Kan R, Kasaba K, Noto K, Muralidhar M, Sakai N and Murakami M 2003 *Physica C* **392–396** 526